Thermo-Optic Multistability and Relaxation in Silicon Microring Resonators with Lateral Diodes

Dodd Gray,[1,*] Ryan Hamerly,[1,†] Meysam Namdari,[2,‡] Mircea-Traian Cătuneanu,[2] Kambiz Jamshidi,[2] Nate Bogdanowicz,[3,§] and Hideo Mabuchi[3]

[1] *Research Laboratory of Electronics, Massachusetts Institute of Technology, 77 Massachusetts Avenue, Cambridge, Massachusetts 02139, USA*

[2] *Integrated Photonic Devices Laboratory, Technische Universität Dresden, Helmholtzstrasse 16, Dresden 01069, Germany*

[3] *Ginzton Laboratory, Stanford University, 348 Via Pueblo Mall, Stanford, California 94305, USA*

(Received 22 March 2020; revised 12 June 2020; accepted 17 June 2020; published 25 August 2020)

We demonstrate voltage-tunable thermo-optic bi- and tristability in silicon photonic microring resonators with lateral *p-i-n* junctions and present a technique for characterizing the thermo-optic transient response of integrated optical resonators. Our method for thermo-optic transient response measurement is applicable to any integrated photonics platform and uses standard equipment. Thermo-optic relaxation in encapsulated waveguides is found to be approximately logarithmic in time, consistent with the analytical solution for two-dimensional heat diffusion. We develop a model for thermo-optic microring multistability and dynamics that agrees with experimental data over a wide range of operating conditions. Our work highlights the fundamental connection in semiconductor waveguides between active free-carrier removal and thermo-optic heating, a result of particular relevance to Kerr soliton-state stability and on-chip frequency-comb generation. The devices studied here are fabricated in a CMOS foundry process and as a result our model is useful for the design of silicon photonic waveguide devices.

DOI: 10.1103/PhysRevApplied.14.024073

I. INTRODUCTION

The microring resonator is a basic building block in integrated photonic systems, providing spectral filtering and resonant interaction enhancement for myriad applications in optical sensing [1], communication [2,3], and information processing [4]. Thermo-optic (TO) coupling, which refers to the temperature dependence of optical materials' refractive indices, plays a prominent role in integrated photonics and optoelectronics. Resistive heating is often used to locally increase the temperature of waveguide materials, in turn altering the phase velocity of guided waves and shifting optical resonances [5–8]. TO tuning also appears as an effective optical nonlinearity in integrated optical waveguides and resonators where absorption of light leads to waveguide heating and can induce resonator multistability [9,10]. TO dynamics of microring resonators must often be considered in the design of integrated optical systems, especially those employing large circulating optical powers or requiring high precision [11–13]. A noteworthy example is the generation of optical frequency combs from continuous-wave (cw) pump lasers, where the ratio of the thermal-relaxation and soliton-formation time scales has been shown to determine whether frequency combs can be stably formed [14]. Experimental characterization of microring thermal relaxation is thus critical for integrated frequency-comb-device design and control [15].

Thermo-optic dynamics are prominent in silicon due to its high TO coefficient and the presence of two-photon absorption (TPA), which leads to carrier generation and heating [9,10,12,16]. Nonlinear losses due to TPA in semiconductor waveguides are compounded with added loss from the plasma formed by TPA-generated free carriers before they diffuse away from the guided optical mode or recombine [17,18]. Extraction of mobile free carriers from waveguides with a reverse-biased *p-i-n* junction [19] can reduce this nonlinear free-carrier absorption (FCA) loss. Such active extraction can reduce the lifetime of carriers by nearly 2 orders of magnitude [20,21], providing access to a wider range of dispersive nonlinear optical regimes [22,23]; however, the electrical work done to extract free carriers also enhances the

*dodd@mit.edu

†Also at NTT Research Inc., East Palo Alto, California 94303, USA.

‡Now at Fraunhofer Institute for Photonic Microsystems, Maria-Reiche-Strasse 2, 01109 Dresden, Germany.

§Now at Entanglement Technologies Inc., 42 Adrian Court, Burlingame, California 94010, USA.

TO effect. Therefore accurate models and characterization techniques for TO dynamics are especially important in silicon photonics.

Here, we present the experimental characterization of TO dynamics and steady-state behavior in silicon microring resonators with lateral *p-i-n* junctions for FC extraction fabricated in a CMOS foundry process. We present a dynamical model for TO nonlinearities in silicon waveguides, compare the fixed points of the model with experimental data, and show that they are in good agreement. As part of this study, we demonstrate a method for measuring thermal relaxation in semiconductor resonators. This technique uses two tunable cw lasers tuned near distant longitudinal resonances of the same microring to pump and probe decaying TO detuning after TO-bistability jumps. This approach builds upon previously demonstrated TO-detuning measurement techniques [24], enabling characterization of transient TO detuning with the use of a spectrally narrow tunable probe. We show that in encapsulated silicon microring resonators, TO detuning is approximately logarithmic in time, consistent with two-dimensional (2D) heat flow from the waveguide core into the surrounding materials [25].

II. DEVICE AND EXPERIMENT

Here, we study thermal relaxation in a silicon lateral-junction microring resonator produced by a multiproject wafer service at a CMOS foundry (IMEC, Belgium) [26]. The microring device is fabricated in the top silicon layer of a silicon-on-insulator (SOI) substrate, directly above a 2-μm buried-oxide (BOX) layer of the SOI substrate, and is encapsulated from above by amorphous silica with approximately 10 μm thickness. The device geometry and quasi-TE_{00} waveguide-mode profile (dominant in-plane *E*-field polarization) are illustrated in Fig. 1(a). The optical resonator is formed by a 40-μm-diameter ring of silicon ridge waveguide with a 215 $\times$ 450 nm cross section and a 70-nm slab height [inset to Fig. 1(a)]. The microring is evanescently coupled to a straight-bus waveguide terminated at both ends with grating couplers. A radial *p-i-n* junction diode is formed across the waveguide by *p*-doping (*n*-doping) the 70-nm silicon cladding inside (outside) the ring; this facilitates carrier extraction for tunable control of the carrier lifetime. Numerical modeling suggests that this waveguide geometry supports both quasi-TE_{00} and quasi-TM_{00} polarized modes near the 1550-nm vacuum

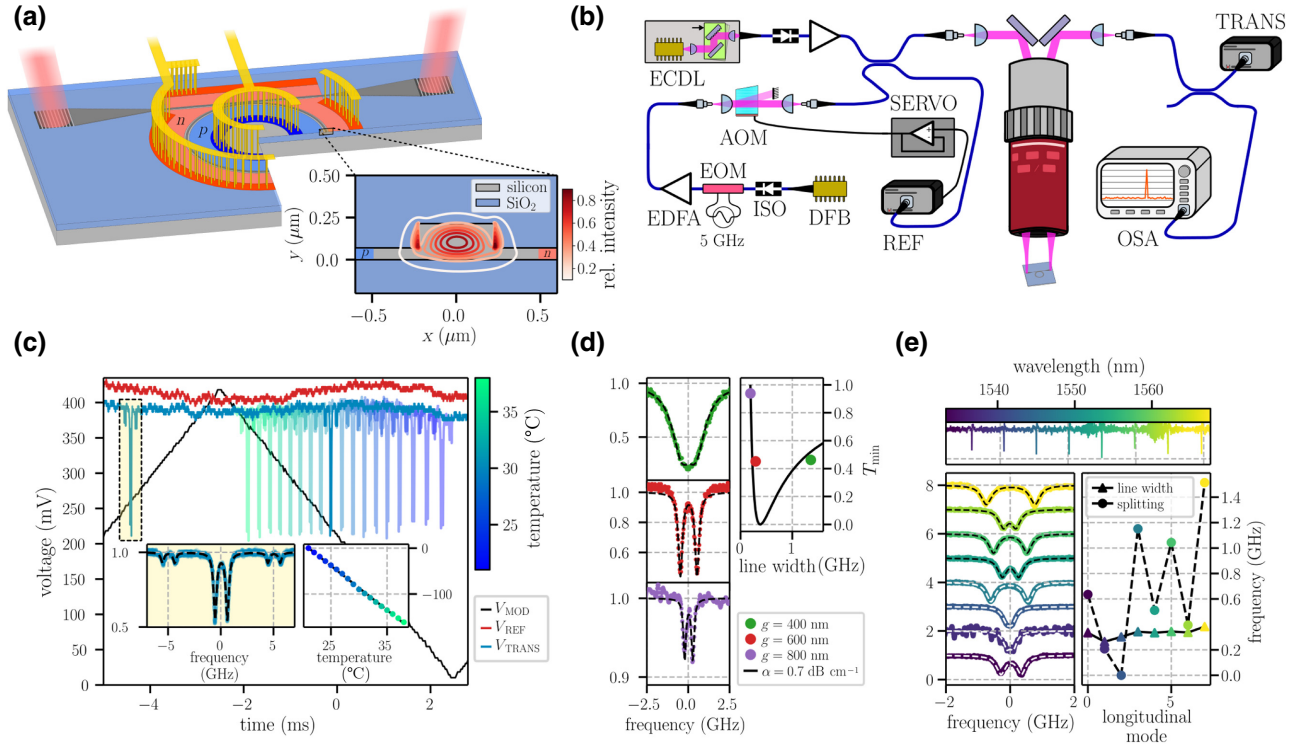

FIG. 1. (a) A schematic depiction of a silicon photonic microring resonator with a lateral *p-i-n* diode for free-carrier extraction. The inset shows the optical-mode intensity profile overlaid on the waveguide cross section. (b) The experiment schematic, discussed in the text. (c) Bus waveguide transmission traces measured at sample temperatures between 15 and 38 °C. The left inset shows an enlarged transmission dip with a doublet profile and sidebands for tuning-rate calibration. The right inset shows linear thermal tuning with a tuning coefficient $\delta_{TO} \approx -9.67\,\mathrm{GHz\,K^{-1}}$. (d) The resonance profiles of identical resonators with varied coupler gaps. (e) The fine structure of eight consecutive longitudinal modes of the same microring, showing large variation in splitting.

wavelength; however, only the quasi-TE_{00} mode is probed in this study.

Figure 1(b) depicts the experimental setup used to characterize this device. The chip is attached to a ceramic chip carrier with silver paint and wire bonded to provide electrical access to the lateral *p-i-n* diode. The chip carrier is placed on a temperature-controlled mount attached to a three-axis translation stage for positioning under a microscope objective for free-space coupling. Two diode-laser sources—an external-cavity diode laser (ECDL, tuning range 1530–1570 nm) and a distributed-feedback laser (DFB) operating near 1550 nm with a 200 GHz (approximately 1.6 nm) mode-hop-free current tuning range—are coupled into the input port after optical isolation with Faraday isolators (ISO) and amplification with erbium-doped fiber amplifiers (EDFAs). The DFB laser power is actively stabilized to enable frequency modulation via current injection at a fixed optical power. This is accomplished using a reference detector (REF) and a servo circuit (SERVO) controlling an acousto-optic modulator (AOM). The DFB is also passed through a 20-GHz electro-optic amplitude modulator (EOM) to enable the addition of known-frequency sidebands for frequency-sweep calibration. Light collected from the output grating is fiber coupled, power split, and simultaneously sent to a transmission photoreceiver (TRANS) and an optical-spectrum analyzer (OSA) for detection. The optical power signals measured by the REF and TRANS photoreceivers are recorded using an oscilloscope. The OSA and oscilloscope, as well as the input light conditioning, sample temperature, and reverse-bias voltage, are all computer controlled with PYTHON code, using the INSTRUMENTAL software package [27].

The linear optical-resonance properties of the microring are initially probed using only the DFB laser with approximately 1 μW optical power coupled into the bus waveguide. With a fixed reverse-bias voltage V_{rb} applied across the ring *p-i-n* diode, transmission spectra are collected by sweeping the DFB frequency over a 180-GHz range using a 30-Hz triangle-wave current modulation. The temperature-dependent bus-waveguide transmission data are shown in Fig. 1(c). The left inset of Fig. 1(c) shows a single resonance-transmission dip with a Lorentzian-doublet line shape and 5-GHz sidebands and the right inset shows the tuning of the resonance center frequency with the sample temperature. Individual resonances are found to have a loaded Q (line width) of 5.4×10^5 (360 MHz) with a TO tuning coefficient $\delta_{TO} \approx -9.67\,\mathrm{GHz\,K^{-1}}$. Spectroscopy of otherwise-identical resonators with varied directional coupler gaps, shown in Fig. 1(d), reveals the intrinsic Q (line width) to be approximately 8.8×10^5 (220 MHz), corresponding to 0.7 $\mathrm{dB\,cm^{-1}}$ waveguide loss in the ring. Line shapes of several consecutive longitudinal resonances of the same device measured using the ECDL are shown in Fig. 1(e). The Lorentzian-doublet splitting is found to vary randomly between 0 and 1.5 GHz from one longitudinal mode to the next on a single device, indicative of roughness-induced standing-wave resonances [28,29]. Compared with the quasi-TE-polarized resonator modes probed here, we expect that the quasi-TM-polarized modes will display somewhat weaker TO coupling. In TM-polarized modes, the electric field is strongly concentrated in the oxide material above and below the waveguide, which has significantly weaker TO coupling [30].

III. TUNABLE THERMO-OPTIC MULTISTABILITY

As the optical input power is increased, voltage (V_{rb})-dependent asymmetric and hysteretic distortion of the resonance line shape due to TO nonlinearity become observable. At $V_{rb} = 0$ V and 15 V, the onset of noticeable TO distortion is at ≥ 80 μW and ≥ 10 μW in the bus waveguide, respectively. The measured TO-resonance distortion and bistability for varied optical power and reverse-bias voltage are shown in Figs. 2(a) and 2(c), respectively. The lateral diode photocurrent I_{pd} is synchronously collected and analyzed. Figure 2(e) shows I_{pd} to vary quadratically with the circulating power P_{circ}. Despite recent reports of dominantly linear-absorption mediated free-carrier generation at 1550 nm up to > 10 mW power levels in similar silicon waveguides [31,32], we do not observe significant linear photocurrent generation down to microwatt levels. Assuming high quantum efficiency of the photocurrent collection, V_{rb} and I_{pd} also enable calculation of the TO heat load $P_{dis} = I_{pd}(V_{rb} + 2\hbar\omega/q)$, where $\hbar\omega \approx 0.8$ eV is the photon energy and q is the electron charge. The on-resonance TO detuning Δ_{TO} and P_{dis} measured for input optical powers of 10–800 μW and reverse-bias voltages of 0–20 V are plotted in Fig. 2(f), along with a linear fit. Note that the vast majority of the resonator-coupled optical power is not included in P_{dis} because it is lost to scatter and does not induce local heating. Interestingly, in this device we observe TO tristability in the regime where Δ_{TO} exceeds the roughness-induced normal-mode splitting, indicated by the presence of three distinct jump positions in the forward- and backward-frequency-sweep data. This is highlighted in Fig. 2(g), which shows transmission and I_{pd} traces when the laser frequency is swept (at fixed power and V_{rb}) across the resonance in both directions and when the sweep is reversed before the bistable jump.

To understand the voltage-tuned TO multistabilities in this device, we use a previously presented model for coupled nonlinearities in microrings [23,33], modified to include two field amplitudes for orthogonal standing-wave modes and with parameters inferred from the linear and TO characterization data shown in Figs. 1 and 2. Measured and calculated phase diagrams showing voltage-tunable regions of TO mono-, bi-, and tristability as functions

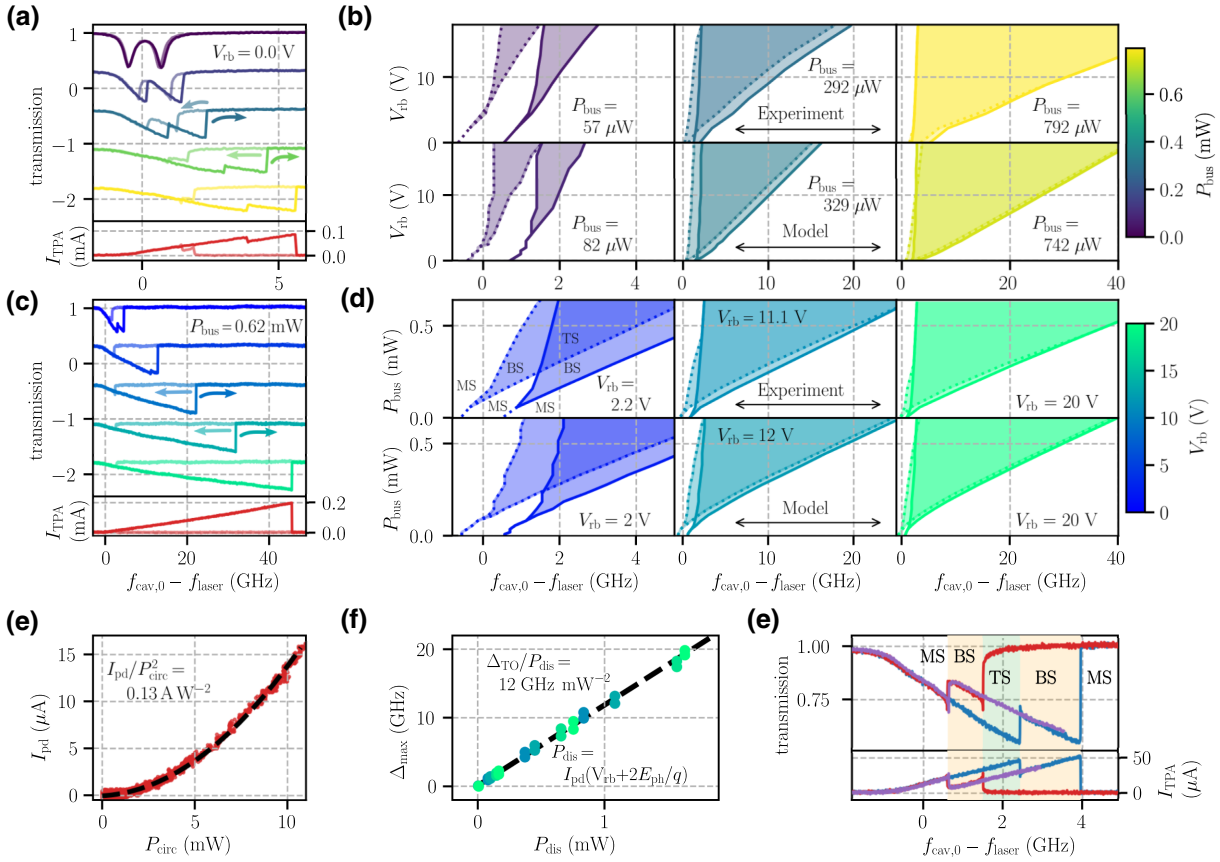

FIG. 2. The (a) power- and (c) voltage-dependent transmission through the bus waveguide, showing voltage-tunable TO bistability. The darker (lighter) curves represent blue-to-red (red-to-blue) laser tuning, as indicated by the arrows. All traces show absolute transmission on the same scale with similar peak extinction of approximately 55%, offset for clarity. The red curves below the transmission plots in (a) and (c) show the lateral diode photocurrent corresponding to the bottom transmission curve. (b),(d) Experimentally measured (top row) and calculated (bottom row) regions of TO multistability as a function of the reverse-bias voltage (b) and the input power (d). Mono-, bi-, and tristability are labeled in (d) as MS, BS, and TS, respectively. Each panel of (b) and (d) corresponds to a fixed value of P_{bus} (V_{rb}), as labeled, and the same color scale is used for P_{bus} in (a) and (b) and V_{rb} in (c) and (d). (e) The measured correspondence between the circulating optical power P_{circ} and the lateral diode photocurrent I_{pd}, with a quadratic fit. (f) The measured TO detuning Δ_{TO} and voltage-controlled power dissipation P_{dis}, with a linear fit. (g) The measured optical transmission and lateral diode current, showing TO tristability. The multistable detuning ranges are labeled as in (d).

of the bus-waveguide-coupled power P_{bus}, the cold-cavity detuning Δ, and the reverse-bias voltage V_{rb} are shown in Figs. 2(b) and 2(d). The model details and the parameter values used are included in Appendix A.

IV. THERMO-OPTIC RELAXATION MEASUREMENT

The bistable jumps seen at high optical powers and reverse-bias voltages enable direct measurement of transient TO relaxation by monitoring the detuning of a different longitudinal mode of the microring with a second weak "probe" laser. Here, the 1550-nm DFB and ECDL sources discussed above are used as the "pump" and the "probe," respectively. A schematic representation, divided into five stages, of the dynamic TO tuning of the microring's longitudinal modes relative to the pump and probe lasers is shown in Fig. 3(b). The ECDL is tuned in steps near a longitudinal mode of the ring at approximately 1530 nm while the DFB frequency was scanned, driving repeatable TO bistable jumps. The transmission data collected for a single value of Δf_{probe} exemplifying this measurement scheme are shown in Fig. 3(a). A 1530-nm optical band-pass filter is used to block pump light at the transmission detector. The timing of the first- and second-probe resonance dips during a single scan indicate, respectively, the cold-cavity detuning of the probe Δf_{probe} and the time delay after the jump before the transient TO detuning falls back to Δf_{probe}. A distinct jump also appears in each transmission trace due to a small fraction of pump light leaking through the band-pass filter. This provides an accurate reference for $t = 0$

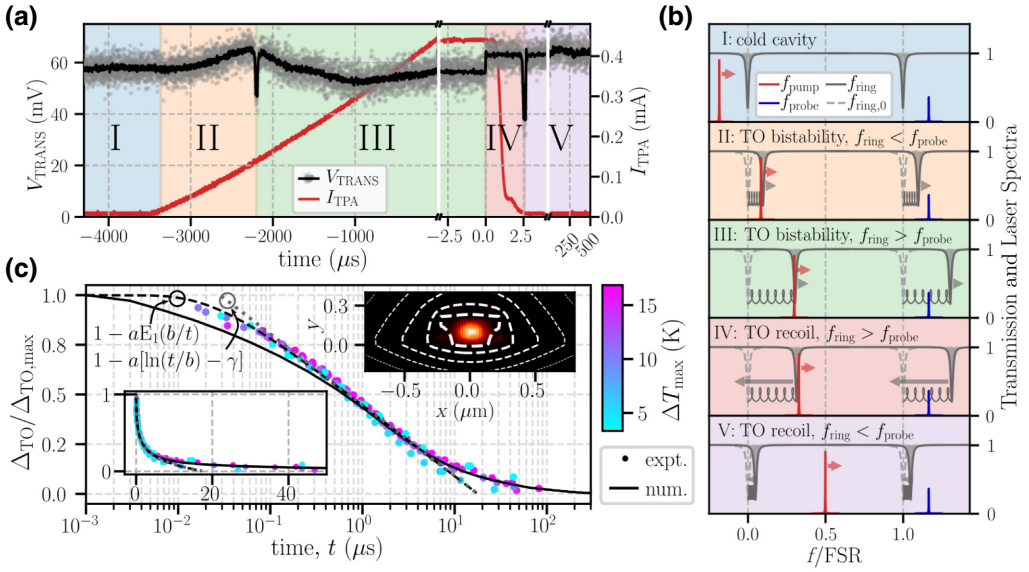

FIG. 3. The direct measurement of microring thermal relaxation with two cw lasers. (a) An example of a trace showing two transmission dips and one small jump in measured with a single photodiode as a strong pump laser is tuned across a microring resonance, inducing TO bistability. The dips result from a longitudinal mode passing a fixed-wavelength probe laser before and after the TO-bistability jump. The delay after the jump as a function of the probe-laser detuning is used to measure the time profile of the thermal relaxation. (b) Schematic spectra showing the evolution of the cavity, pump, and probe-laser spectra through the five labeled stages in (a). (c) The measured, numerically modeled, and fitted analytical time profiles of microring TO relaxation, normalized to the initial temperature deflection. The thermal relaxation is approximately logarithmic in time for 100-ns–10-μs time delays, as discussed in the text. Relaxation from temperature deflections from ambient between 4 and 16 K are measured, as indicated by the color bar on the right. The insets show the same data plotted on a linear time scale and the initial temperature distribution around the optical-mode profile.

(the jump time) within a single trace. The synchronously recorded transverse diode current [also shown in Fig. 3(a)] is consistent with this interpretation of the transmission data.

Relaxation of the microring waveguide temperature deflection $\Delta T(t)$, inferred from the probe resonance detuning, is measured over nearly 4 orders of magnitude in time delay after the jump (between 20 ns and 80 μs) with a temperature resolution of 0.1 K using different cold-cavity detuning values of the probe laser. The pump power is varied to control ΔT_{max}, the waveguide temperature deflection at the time of the jump. Measurements are performed with $V_{rb} = 15$ V to simultaneously maximize the achievable waveguide temperature deflection and minimize the impact of free carriers. Relaxation of the microring waveguide temperature after a TO-bistability jump is observed to decay with an approximately logarithmic time dependence, in agreement with 2D numerical simulations of TO tuning from TPA-proportional heating in these waveguides as well as previous studies of transient heating in optical tweezers [34]:

$$\Delta T(t) \approx 1 - aE_1(b/t) \tag{1}$$

$$\approx 1 - a\left[\ln(t/b) - \gamma\right], \tag{2}$$

where $E_1(x) = \int_x^\infty (e^{-x}/x)dx$ is the exponential integral function, t is the time after the bistability jump, $\gamma \approx 0.577$ is the Euler-Mascheroni constant, and $a = 0.155$ and $b = 16$ ns are constants determined by fitting to experimental data in Fig. 3(b) encoding the heat capacity and thermal conductivity of the media surrounding the waveguide. $E_1(x)$ is approximated with a truncated series expansion in Eq. (2). This TO-relaxation time dependence is expected for 2D radial heat transfer from a point source (the waveguide cross section) into the distributed heat capacity of the surrounding medium [25], as discussed in Appendix B.

V. CONCLUSIONS

We measure and model TO effects in CMOS silicon microring resonators with lateral p-i-n junctions for active free-carrier removal. Our results highlight the fact that active free-carrier removal comes with the side effect of increased TO nonlinearity caused by Joule heating and we demonstrate a voltage-tunable TO response that is potentially useful for a variety of waveguide devices that require thermal control. We map out measured regions of TO multistability in our device and specify a model for the TO dynamics that shows good agreement and that can be used for future photonic device design in similar platforms.

The demonstrated voltage-tunable increase in TO response can be viewed as a resource, providing a means of low-power, high-bandwidth electronic control over *in situ* laser heating of the optical-mode volume in a microring resonator. TO tuning of photonic resonators with "auxiliary" laser light has been shown to provide robust access to single-soliton states in microring Kerr combs [35,36] and has been explored in a variety of optical media [37,38]. While temperature control with guided laser light offers advantages in response time and power efficiency over conventional displaced electronic heaters, it requires large optical powers and is generally incompatible with semiconductor microrings, where free carriers generated by TPA of the auxiliary laser will add significant loss for all resonator modes. The reverse-bias regime explored here simultaneously reduces the laser power required for TO tuning to the microwatt scale and the free-carrier lifetime to 10 ps, rendering nonlinear FC losses insignificant. This suggests that a hybrid electro-optic approach that directly heats the optical-mode volume without added loss and is voltage tunable may be viable for semiconductor waveguides.

We demonstrate a method of measuring the time profile of thermal relaxation in microring resonators using an auxiliary cw laser as a probe of dynamic detuning after TO-bistability jumps. This relatively simple and low-cost measurement technique is applicable for general characterization of TO dynamics in integrated optical waveguides. We show TO relaxation of silicon microrings fabricated in a standard CMOS process to be approximately logarithmic in time, a result of the quasi-2D nature of radial heat transfer from the waveguide into the surrounding materials, with the majority of cooling occurring in the first 1–2 μs and a long tail extending to nearly 80 μs. This measurement also highlights the potential for CMOS microrings as optically addressable thermometers with high temporal and temperature resolution, potentially useful for monitoring thermal dynamics in proximate microscopic (e.g., biological) systems. Fabrication in a CMOS foundry process also provides for scalable arrays of sensors addressable via a single optical fiber with integrated detection and electronic signal processing.

ACKNOWLEDGMENTS

This work is supported in part by the German Research Foundation (DFG Grant No. JA 2401/11) and by the National Science Foundation (Grant No. PHY-1648807).

APPENDIX A: CAVITY MULTISTABILITY MODEL

The thermo-optic (TO) multistability of the silicon microring resonator is modeled using the following set of coupled ordinary differential equations (ODEs), adapted from recent work studying free-carrier oscillations (FCO) and Kerr-comb generation [23,33]. In this model, linearly orthogonal standing-wave modes with complex amplitudes a_s and a_c (for "sine" and "cosine") couple via two-photon abosorption (TPA) to a free-carrier population with density n and temperature deflection from ambient T. The set of coupled ODEs is written in terms of unitless field, free-carrier density, and temperature quantities $\bar{a}_i = a_i/\xi_a$, $\bar{n} = n/\xi_n$, and $\bar{T} = T/\xi_T$ normalized to reflect the strengths of the Kerr, FCA, and TO nonlinear optical coupling, respectively [23,33]:

$$\frac{d\bar{a}_c}{d\bar{\tau}} = \left[\left(-\frac{1}{2} + i\left[\bar{\Delta}_0 - \frac{\bar{\delta}_r}{2}\right]\right) + (i-r)\left(|\bar{a}_c|^2 + \tfrac{2}{3}|\bar{a}_s|^2\right) + \left(-i-\mu^{-1}\right)\bar{n}_c + i\bar{T}\right]\bar{a}_c + \sqrt{\eta}\bar{a}_{\text{in}}, \tag{A1}$$

$$\frac{d\bar{a}_s}{d\bar{\tau}} = \left[\left(-\frac{1}{2} + i\left[\bar{\Delta}_0 + \frac{\bar{\delta}_r}{2}\right]\right) + (i-r)\left(|\bar{a}_s|^2 + \tfrac{2}{3}|\bar{a}_c|^2\right) + \left(-i-\mu^{-1}\right)\bar{n}_s + i\bar{T}\right]\bar{a}_s + \sqrt{\eta}\bar{a}_{\text{in}}, \tag{A2}$$

$$\frac{d\bar{n}}{d\bar{\tau}} = -\frac{\bar{n}}{\bar{\tau}_{\text{fc}}} + \chi\left(|\bar{a}_c|^4 + \frac{4}{3}|\bar{a}_c|^2|\bar{a}_s|^2 + |\bar{a}_s|^4\right), \tag{A3}$$

$$\frac{d\bar{T}}{d\bar{\tau}} = -\frac{\bar{T}}{\bar{\tau}_{\text{th}}} + \zeta\left[\phi\chi\left(|\bar{a}_c|^4 + \frac{4}{3}|\bar{a}_c|^2|\bar{a}_s|^2 + |\bar{a}_s|^4\right) + \frac{\chi\bar{n}}{\mu r}\left(|\bar{a}_c|^2 + |\bar{a}_s|^2\right),\right] \tag{A4}$$

where the time scale is normalized to the photon lifetime ($\bar{\tau} = t/\tau_{\text{ph}}$), $\bar{\Delta}_0 \pm \bar{\delta}_r/2 = (\omega_{\text{laser}} - \omega_{\text{cav}})\tau_{\text{ph}}$ are the cold-cavity detunings measured in resonance line widths, and $\bar{\delta}_r = 2\pi\delta_r\tau_{\text{ph}}$ is the line-width-normalized normal-mode splitting due to backscattering in the waveguide ring resonator. The unitless parameters χ and ζ are normalized coefficients for the free-carrier dispersion (FCD) and TO coupling coefficients, while r and μ account for the Kerr-to-TPA and FCD-to-FCA nonlinearity strength ratios, respectively. The free carriers and temperature deflections decay on time scales of $\bar{\tau}_{\text{fc}}$ and $\bar{\tau}_{\text{th}}$, respectively. The free-carrier lifetime τ_{fc} and the dissipation-per-absorption parameter ϕ depend on V_{rb} as follows:

$$\phi = \frac{qV_{\text{rb}} + 2\hbar\omega}{2\hbar\omega}, \tag{A5}$$

$$\tau_{\text{fc}} \approx \left(\tau_{\text{fc},0} - \tau_{\text{fc,sat}}\right)e^{-V_{\text{rb}}/V_{\tau_{\text{fc}}}} + \tau_{\text{fc,sat}}, \tag{A6}$$

where $\hbar\omega$ is the photon energy (0.8 eV at 1550 nm), $\tau_{\text{fc},0}$ is the free-carrier lifetime for $V_{\text{rb}} = 0$ (short-circuit

condition), $\tau_{\mathrm{fc,sat}}$ is the minimal free-carrier lifetime limited by velocity saturation, and $V_{\tau_{\mathrm{fc}}}$ is a fit parameter for the approximately exponential dependence of τ_{fc} on V_{rb} seen in experiment [19] and simulation [23]. Assuming efficient free-carrier collection from the undoped waveguide, the lateral photodiode current is proportional to the electron-hole pair generation rate

$$I_{\mathrm{pd}} = \xi_I \chi \left(|\bar{a}_c|^4 + \frac{4}{3}|\bar{a}_c|^2|\bar{a}_s|^2 + |\bar{a}_s|^4 \right), \tag{A7}$$

$$\xi_I = \frac{q v_m \xi_n}{2\tau_{\mathrm{ph}}}, \tag{A8}$$

where $v_m = \pi d_{\mathrm{ring}} A_{\mathrm{eff}}$ is the mode volume. For our device parameters, the current normalization is $\xi_I \approx 5.9\ \mu$A. When the normal mode splitting exceeds the resonance line width, we expect two-photon absorption by the individual standing-wave modes to dominate the cross-coupling, such that $\left(|\bar{a}_c|^4 + |\bar{a}_s|^4\right) \gg \frac{4}{3}|\bar{a}_c|^2|\bar{a}_s|^2$ in Eqs. (A3) and (A7). Equation (A7) provides a robust relationship between the measured photocurrent and optical power circulating in the microring because the device geometry, the resonance line width, and the material parameters that determine ξ_n are all precisely characterized. Determination of the intracavity power from the photocurrent has the benefit of being alignment insensitive, which is particularly useful in our experimental setup, where we observe that the grating coupler efficiencies drift slowly over time. Thus I_{pd} is used to calibrate the instantaneous intracavity and bus-coupled optical powers P_{circ} and $P_{\mathrm{bus}} = \eta P_{\mathrm{circ}}/2$ reported in the main text. The factor of 2 in the preceding relation appears because the standing-wave resonances are excited unidirectionally, while each couples equally to forward- and backward-propagating waves in the bus waveguide.

TABLE I. The normalization coefficients, definitions, and relevant device and bulk-silicon material parameters needed for the TO-multistability model given in Eqs. (A1)–(A4). The device parameters are taken from experimental data as discussed in the text. Citations for the bulk-silicon material parameters are provided in previous work [23].

Parameter	Symbol		Definition	Value
Normalization constants				
Circulating field	ξ_a	=	$\left[\gamma v_g \tau_{\mathrm{ph}}\right]^{-1/2}$	7913 $^{1/2}$ cm^{-1}
Input-output field	ξ_{in}	=	$\left[\gamma v_g \tau_{\mathrm{ph}}^2 t_R^{-1}\right]^{-1/2}$	478 W$^{1/2}$ cm^{-1}
Free-carrier density	ξ_n	=	$2/\left(\mu\sigma v_g \tau_{\mathrm{ph}}\right)$	1.3×10^{15} cm^{-3}
Temperature deflection	ξ_T	=	$\left[\delta_{\mathrm{TO}} v_g \tau_{\mathrm{ph}}\right]^{-1}$	36 mK
Diode current	ξ_I	=	$\frac{\pi d_{\mathrm{ring}} A_{\mathrm{eff}}}{2} \frac{q\xi_n}{\tau_{\mathrm{ph}}}$	5.9 μA
Normalized coefficients				
TPA-to-SPM strength ratio	r	=	$\frac{\beta}{2\gamma}$	0.19
FCD-to-FCA strength ratio	μ	=	$\frac{4\pi}{\lambda} \frac{\lvert dn_{\mathrm{si}}/dn_c \rvert}{d\alpha_{\mathrm{si}}/dn_c}$	30
TPA FC-generation coefficient	χ	=	$(r\mu\sigma)\,/\,(2\hbar\omega\gamma v_g)$	13.8
TO tuning coefficient	ζ	=		0.47
Device and material parameters				
Photon lifetime	τ_{ph}	=	$2\pi/\mathrm{FWHM}$	455 ps
Maximum FC lifetime	$\tau_{\mathrm{fc,0}}$	=		140 ps
Minimum FC lifetime	$\tau_{\mathrm{fc,sat}}$	=		3.1 ps
FC-lifetime decay constant	$V_{\tau_{\mathrm{fc}}}$	=		2.15 V
TO decay time	τ_{th}	=		30 ns
Round-trip time	t_R	=	$\frac{\pi d_{\mathrm{ring}}}{v_g} = 1/\mathrm{FSR}$	1.7 ps
Normal-mode splitting	δ_r	=		1.1 GHz
TO tuning coefficient	δ_{TO}	=		-9.7 GHz K^{-1}
Ring-bus power coupling	θ	=		1.6×10^{-3}
Mode effective area	A_{eff}	=		1.0×10^{-9} cm^2
Modal-group index	$n_{g,\mathrm{eff}}$	=	c/v_g	3.97
Ring diameter	d_{ring}	=		40 μm
Photon energy	$\hbar\omega$	=		0.8 eV
SPM coefficient	γ	=	$\frac{2\pi}{\lambda} n_2$	3.1×10^{-9} cm W^{-1}
FCA cross section	σ	=		1.45×10^{-17} cm^2

Even at moderate reverse-bias voltages $V_{\rm rb} > 1$ V, in our device we expect $\tau_{\rm fc} \ll \tau_{\rm ph}$, rendering FCA and FCD insignificant compared to the enhanced TO response. In this limit, the TO shift $\Delta_{\rm TO} = \xi_T \bar{T} \delta_{\rm TO}$ is proportional to the dissipated power $P_{\rm dis} = I_{\rm pd}\,(V_{\rm rb} + 2\hbar\omega/q)$. From these definitions and Eqs. (A4)–(A8), we find that in steady state,

$$\Delta_{\rm TO} \approx \xi_T\,(\bar{\tau}_{\rm th}\zeta)\,\frac{r\phi}{\chi}\,\frac{I_{\rm pd}}{\xi_I} \tag{A9}$$

$$= (\bar{\tau}_{\rm th}\zeta)\,\frac{\xi_T}{\xi_I}\,\frac{\delta_{\rm TO}}{2\hbar\omega/q} P_{\rm dis}. \tag{A10}$$

As expected, $\Delta_{\rm TO}$ and $P_{\rm dis}$ are measured to be proportional in experiment [see Fig. 2(f) in the main text] with a ratio $\Delta_{\rm TO}/P_{\rm dis} \approx 12\ {\rm GHz\,mW^{-1}}$. According to Eq. (A10), we infer that $\bar{\tau}_{\rm th}\zeta \approx 16.3$.

With the exception of $\tau_{\rm fc,0}$, all device-dependent parameters needed for steady-state solutions of these equations are determined from the experimental data presented in Figures 1 and 2 of the main text. A finite-element model (LUMERICAL DEVICE) is used to estimate $\tau_{\rm fc,0}$ and $\tau_{\rm fc}(V_{\rm rb})$ with an empirical exponential fit, consistent with previous experimental and numerical studies of similar waveguides [19,20]. The parameter values and normalization coefficients ξ_i are provided in Table I. Citations for bulk-silicon material parameters are provided in previous work [23].

The steady-state solutions of Eqs. (A1)–(A4) [along with the complex conjugates of Eqs. (A1)–(A2)] reduce to a simultaneous pair of seventh-order polynomial equations in $|\bar{a}_c|^2$ and $|\bar{a}_s|^2$, which is solved numerically using MATHEMATICA in the experimentally accessible parameter range. The stability of the fixed points is determined from the locations in the complex plane of the ODE system's Jacobian eigenvalues. The white, light-shaded, and dark-shaded regions in Fig. 2(d) of the main text, respectively labeled MS, BS, and TS, indicate the parameter regimes in which one, two, and three stable solutions are found.

APPENDIX B: LOGARITHMIC THERMO-OPTIC RELAXATION

A simplified model can be used to understand the time dependence of the thermal transients in this system. We consider the step-function transient response of the 2D heat equation to a point heat source at the origin:

$$\left[\nabla^2 - \frac{1}{\alpha}\frac{\partial}{\partial t}\right]\Delta T(r,t) = -\frac{Q(r,t)}{\kappa}, \tag{B1}$$

$$Q(r,t) = Q_0\delta(r)\Theta(t), \tag{B2}$$

where $\alpha = \kappa/(\rho c_p)$ is the thermal diffusivity, κ is the thermal conductivity, ρ is the density, c_p is the heat capacity, Q_0 is the linear power density of the heat source, $\delta(r)$ is the Dirac δ function at the origin, and $\Theta(t)$ is the Heaviside step function indicating that the heat source is turned on at time $t = 0$. For concreteness, we note that $Q_0 = P_{\rm dis}/(\pi d_{\rm ring})$ in the context of microring heating by guided light. The solution for the temperature-deflection transient $\Delta T(r,t)$ can be expressed as an exponential integral function E_1:

$$\Delta T(r,t) = \frac{Q_0}{4\alpha}\int_{\frac{r^2}{4\alpha t}}^{\infty}\frac{e^{-z}}{z}dz \tag{B3}$$

$$= \frac{Q_0}{4\alpha}\mathrm{E}_1\left(\frac{r^2}{4\alpha t}\right) \tag{B4}$$

$$\overset{t\gg r^2/4\alpha}{\longrightarrow} \frac{Q_0}{4\alpha}\left[-\gamma - \ln\left(\frac{r^2}{4\alpha t}\right)\right], \tag{B5}$$

where $\mathrm{E}_1(x) = \int_x^\infty (e^{-x}/x)dx$ is the exponential integral function, $\gamma \approx 0.577$ is the Euler-Mascheroni constant, and in Eq. (B5) $\mathrm{E}_1\left[r^2/(4\alpha t)\right]$ is approximated by a truncated Puiseux series along the real axis [39], valid in the limit $t \gg r^2/4\alpha$. We consider an approximately Gaussian transverse mode of an optical waveguide centered at the origin with waist w_0. $\Delta T(r,t)$ is sampled by waveguide modes to determine the transient TO perturbation. The point-source approximation made in Eq. (B2) is self consistent at times $t \gtrsim w_0^2/(4\alpha)$ when $\Delta T(r,t)$ is approximately constant over the mode intensity profile. From Eq. (B5), we expect that in this regime the transient temperature deflection overlapping the optical mode can be approximated as

$$\Delta T(t) \approx 1 - a\mathrm{E}_1(b/t), \tag{B6}$$

$$\approx 1 - a\,[\ln(t/b) - \gamma], \tag{B7}$$

where $a = 0.155$ and $b = 16$ ns are constants determined by fitting to experimental data in Fig. 3(b) that depend on the waveguide geometry and the heat capacity, thermal conductivity, and refractive indices of the core and cladding materials. In a microring with diameter $d_{\rm ring}$, this 2D heat-transfer model will remain valid for times $t \lesssim d_{\rm ring}^2/(16\alpha)$. From the modal effective area $A = 0.1\ \mu{\rm m}^2$ and the thermal diffusivity of amorphous silica $\alpha_{a-{\rm SiO_2}} = 9\times10^{-3}\ {\rm cm^2/s}$, we can estimate the transient TO step response to have the form of Eq. (2) for 10 ns $\lesssim t \lesssim$ 100 μs. This rough estimate provides a reasonable prediction of the experimentally observed TO step response shown in Fig. 3(b); however, it neglects heat conduction by the 60-nm-thick crystalline silicon cladding in the plane of the microring and numerous other features of the device geometry. We use a finite-element model (LUMERICAL

DEVICE) to account for these aspects and still find a logarithmic transient consistent with Eq. (2). Our numerical model suggests that the high thermal diffusivity of the thin silicon cladding layer ($\alpha_{si} = 0.8\ cm^2/s$) can account for the experimentally observed deviation from the logarithmic time dependence near $t = 10\ \mu s$ [Fig. 3(b)].

[1] P. Trocha, M. Karpov, D. Ganin, M. H. P. Pfeiffer, A. Kordts, S. Wolf, J. Krockenberger, P. Marin-Palomo, C. Weimann, S. Randel, W. Freude, T. J. Kippenberg, and C. Koos, Ultrafast optical ranging using microresonator soliton frequency combs, Science **359**, 887 (2018), publisher: American Association for the Advancement of Science Section: Report.

[2] J. Pfeifle, V. Brasch, M. Lauermann, Y. Yu, D. Wegner, T. Herr, K. Hartinger, P. Schindler, J. Li, D. Hillerkuss, R. Schmogrow, C. Weimann, R. Holzwarth, W. Freude, J. Leuthold, T. J. Kippenberg, and C. Koos, Coherent terabit communications with microresonator Kerr frequency combs, Nat. Photonics **8**, 375 (2014).

[3] C. Sun *et al.*, Single-chip microprocessor that communicates directly using light, Nature **528**, 534 (2015).

[4] Y. Okawachi, M. Yu, X. Ji, J. K. Jang, M. Lipson, and A. L. Gaeta, in *Conference on Lasers and Electro-Optics* (Optical Society of America, 2019), p. FM1D.6.

[5] R. Espinola, M. Tsai, J. Yardley, and R. Osgood, Fast and low-power thermooptic switch on thin silicon-on-insulator, IEEE Photonics Technol. Lett. **15**, 1366 (2003).

[6] M. Harjanne, M. Kapulainen, T. Aalto, and P. Heimala, Sub-μs switching time in silicon-on-insulator Mach-Zehnder thermooptic switch, IEEE Photonics Technol. Lett. **16**, 2039 (2004).

[7] T. Chu, H. Yamada, S. Ishida, and Y. Arakawa, Compact $1 \times N$ thermo-optic switches based on silicon photonic wire waveguides, Opt. Express **13**, 10109 (2005).

[8] A. H. Atabaki, A. A. Eftekhar, S. Yegnanarayanan, and A. Adibi, Sub-100-nanosecond thermal reconfiguration of silicon photonic devices, Opt. Express **21**, 15706 (2013).

[9] I. D. Rukhlenko, M. Premaratne, and G. P. Agrawal, Analytical study of optical bistability in silicon-waveguide resonators, Opt. Express **17**, 22124 (2009).

[10] I. D. Rukhlenko, M. Premaratne, and G. P. Agrawal, Analytical study of optical bistability in silicon ring resonators, Opt. Lett. **35**, 55 (2010).

[11] T. Carmon, L. Yang, and K. J. Vahala, Dynamical thermal behavior and thermal self-stability of microcavities, Opt. Express **12**, 4742 (2004).

[12] T. J. Johnson, M. Borselli, and O. Painter, Self-induced optical modulation of the transmission through a high-Q silicon microdisk resonator, Opt. Express **14**, 817 (2006).

[13] M. de Cea, A. H. Atabaki, and R. J. Ram, Power handling of silicon microring modulators, Opt. Express **27**, 24274 (2019).

[14] Q. Li, T. C. Briles, D. A. Westly, T. E. Drake, J. R. Stone, B. R. Ilic, S. A. Diddams, S. B. Papp, and K. Srinivasan, Stably accessing octave-spanning microresonator frequency combs in the soliton regime, Optica **4**, 193 (2017).

[15] C. Joshi, J. K. Jang, K. Luke, X. Ji, S. A. Miller, A. Klenner, Y. Okawachi, M. Lipson, and A. L. Gaeta, Thermally controlled comb generation and soliton modelocking in microresonators, Opt. Lett. **41**, 2565 (2016).

[16] I. A. Temnykh, N. F. Baril, Z. Liu, J. V. Badding, and V. Gopalan, Optical multistability in a silicon-core silica-cladding fiber, Opt. Express **18**, 5305 (2010).

[17] R. Soref and B. Bennett, Electrooptical effects in silicon, IEEE J. Quantum Electron. **23**, 123 (1987).

[18] T. K. Liang and H. K. Tsang, Role of free carriers from two-photon absorption in Raman amplification in silicon-on-insulator waveguides, Appl. Phys. Lett. **84**, 2745 (2004), publisher: American Institute of Physics.

[19] A. C. Turner-Foster, M. A. Foster, J. S. Levy, C. B. Poitras, R. Salem, A. L. Gaeta, and M. Lipson, Ultrashort free-carrier lifetime in low-loss silicon nanowaveguides, Opt. Express **18**, 3582 (2010).

[20] A. Gajda, L. Zimmermann, J. Bruns, B. Tillack, and K. Petermann, Design rules for *p-i-n* diode carriers sweeping in nano-rib waveguides on SOI, Opt. Express **19**, 9915 (2011).

[21] M. Sen, T. Datta, and M. K. Das, in *2013 International Conference on Microwave and Photonics (ICMAP)* (2013), p. 1.

[22] M. Yu, Y. Okawachi, A. G. Griffith, M. Lipson, and A. L. Gaeta, Mode-locked mid-infrared frequency combs in a silicon microresonator, Optica **3**, 854 (2016).

[23] R. Hamerly, D. Gray, C. Rogers, and K. Jamshidi, Conditions for parametric and free-carrier oscillation in silicon ring cavities, J. Lightwave Technol. **36**, 4671 (2018).

[24] M. Bernard, F. R. Manzano, L. Pavesi, G. Pucker, I. Carusotto, and M. Ghulinyan, Complete crossing of Fano resonances in an optical microcavity via nonlinear tuning, Photonics Res. **5**, 168 (2017).

[25] J. C. Jaeger and H. S. Carslaw, *Conduction of Heat in Solids* (Clarendon Press, New York, 1959).

[26] P. P. Absil, P. De Heyn, H. Chen, P. Verheyen, G. Lepage, M. Pantouvaki, J. De Coster, A. Khanna, Y. Drissi, and D. Van Thourhout, in *Silicon Photonics X* (International Society for Optics and Photonics, San Francisco, 2015), Vol. 9367, p. 93670V.

[27] N. Bogdanowicz, Instrumental, Zenodo (2018). mabuchi-lab/Instrumental: 0.5, version 0.5, http://doi.org/10.5281/zenodo.2556399.

[28] D. S. Weiss, V. Sandoghdar, J. Hare, V. Lefèvre-Seguin, J.-M. Raimond, and S. Haroche, Splitting of high-Q Mie modes induced by light backscattering in silica microspheres, Opt. Lett. **20**, 1835 (1995).

[29] E. S. Hosseini, S. Yegnanarayanan, A. H. Atabaki, M. Soltani, and A. Adibi, High quality planar silicon nitride microdisk resonators for integrated photonics in the visible wavelength range, Opt. Express **17**, 14543 (2009).

[30] J. Komma, C. Schwarz, G. Hofmann, D. Heinert, and R. Nawrodt, Thermo-optic coefficient of silicon at 1550 nm and cryogenic temperatures, Appl. Phys. Lett. **101**, 041905 (2012).

[31] A. Gil-Molina, I. Aldaya, J. L. Pita, L. H. Gabrielli, H. L. Fragnito, and P. Dainese, Optical free-carrier generation in silicon nano-waveguides at 1550 nm, Appl. Phys. Lett. **112**, 251104 (2018).

[32] P. Dainese, I. Aldaya, A. Gil-Molina, L. H. Gabrielli, H. L. Fragnito, and J. L. Pita, in *Optical Interconnects XIX* (International Society for Optics and Photonics, San Francisco, 2019), Vol. 10924, p. 1092412.

[33] R. Hamerly, D. Gray, C. Rogers, L. Mirzoyan, M. Namdari, and K. Jamshidi, in *Physics and Simulation of Optoelectronic Devices XXV* (International Society for Optics and Photonics, San Francisco, 2017), Vol. 10098, p. 100980D.

[34] P. M. Celliers and J. Conia, Measurement of localized heating in the focus of an optical trap, Appl. Opt. **39**, 3396 (2000).

[35] Y. Geng, M. L. Liao, H. Zhou, B. J. Wu, and K. Qiu, in *Nonlinear Optics (2017), paper NM1A.4* (Optical Society of America, Waikoloa Hawaii, 2017), p. NM1A.4.

[36] S. Zhang, J. M. Silver, L. D. Bino, F. Copie, M. T. M. Woodley, G. N. Ghalanos, A. Ø. Svela, N. Moroney, and P. Del'Haye, Sub-milliwatt-level microresonator solitons with extended access range using an auxiliary laser, Optica **6**, 206 (2019).

[37] S. Tenenbaum and R. R. Panepucci, in *2018 SBFoton International Optics and Photonics Conference (SBFoton IOPC)* (Campinas Brazil, 2018), p. 1.

[38] P. Hill, C. Klitis, B. Guilhabert, M. Sorel, E. Gu, M. D. Dawson, and M. J. Strain, All-optical tuning of a diamond micro-disk resonator on silicon, Photonics Res. **8**, 318 (2020).

[39] N. J. A. Sloane, *A Handbook of Integer Sequences* (Academic Press, New York, 2014).